Analysis of the geometrical imperfections of a dry-stacked masonry block based on Miscanthus

Patrick Pereira Dias, Vanessa Jesuino Kammer, Danièle Waldmann *

Faculty of Science, Technology and Medicine (FSTM), University of Luxembourg, 6 Avenue de la Fonte, Esch-sur-Alzette L-4364, Luxembourg

A R T I C L E   I N F O

A B S T R A C T

This paper aims to verify the suitability of masonry blocks based on Miscanthus concrete to be used in dry-stacked walls. Therefore, the load-bearing capacity of single Miscanthus concrete masonry blocks as well as of dry-stacked wallets based on these blocks is analysed in function of geometrical imperfections, such as possible height differences between adjacent blocks due to the production process or/and surface roughness of the dry bed joint. For the study on the load-bearing capacity of single masonry blocks the mixture composition was varied and optimised leading to a maximum ultimate load of 5.42 MPa. With the optimised mixture composition masonry blocks were produced to create small wallets, which achieved a maximum load-bearing capacity of 4.84 MPa. The Miscanthus masonry blocks presented a low Young's Modulus leading to a very ductile behaviour of the wallet without sudden failure. Furthermore, the variation of the contact area as a consequence of geometrical imperfections was studied and an exponential relation between the contact area and the applied load could be established.

1. State of the art

The need for a sustainable building is rising more and more to reduce the enormous energy consumption rates and CO_2 emissions provoked by the construction sector. According to the Global Alliance for Buildings and Construction, the construction sector is responsible for 36% of the energy use and 39% of the CO_2 emissions in the world [1–4]. Numerous measures have been studied to reduce these rates and simultaneously reduce the usage of non-renewable resources such as natural sand and gravel, which are consecutively decreasing due to their substantial exploitation [5]. The latter can be attained by replacing these natural resources with a sustainable plant-based material that has good thermal and acoustic properties [6–8]. Applying Miscanthus like bioenergy crop, which can grow on industrially contaminated grounds [9–11], on a dry-stacked masonry system would reduce the usage of mortar, which implies reduced energy consumption and carbon emissions [12].

The C_4-plant Miscanthus has a wide range of genotypes, and its origins are from East Asia [13,14]. Due to its capacity to grow under a vast range of climatic conditions [15], Aksel Olsen introduced the Miscanthus $\times$ giganteus (MxG) grass from Japan to Europe in the 1930s [13]. MxG plant grows a height of up to 4 m and it shows carbon neutrality. It also has little or no yield response to fertiliser and

pesticides applications. Due to these advantages, MxG shows a positive yield response economically and ecologically [16–18]. Besides, MxG can grow on contaminated soil and simultaneously improving it by reducing its contamination, which increases its fertility [19,20]. Furthermore, the water use of MxG results in a surface stabilisation of the soil, which impedes soil erosion, metal transportation due to wind and water movement [19].

Due to its high yield potential, MxG plant is mostly used for bioenergy production for direct combustion, gasification or as chopped material [21,22]. MxG is also applied as an oil binding material, in agriculture, e.g. as mulch or bedding for animals, mulch for pathways and in the construction sector [23]. Pude et al. [24] analysed the suitability of the fibres of MxG and three other Miscanthus genotypes (Miscanthus sacchariflorus, Miscanthus sinensis and Miscanthus Robustus) used as a filler for lightweight concrete and investigated the achieved compressive strength. According to Pude et al. [24], the highest compressive strength was obtained with the genotype MxG due to its high cellulose content and its high binding capacities of water in the concrete matrix. Furthermore, according to Godard et al. and Wang et al. [25,26], the cost competitiveness of the usage of MxG as a filler could be increased by diminishing the transport distances of this material. This decrease could be achieved by encouraging local farming,

which implies a reduction in CO_2 emissions and benefits the local economy.

The use of a dry-stacked system instead of a conventional system would be an economical way of constructing a wall in a building. The main difference between these two systems is that no mortar is used in the vertical and horizontal joints in the dry-stacked system. As a result, the working speed of labour is increased since there is no need to lay the mortar or wait for it to dry, so the next layer of masonry blocks can be applied [27,28]. Consequently, various interlocking systems, which can be classified as geometric or non-geometric mechanisms [27], have been developed by many researchers. The first holds due to its geometry, which can be a dovetail connection between the blocks or a tongue and groove arrangement or a post-tensioned technique [29]. The second one holds due to a post-treatment on a wall, which can be due to grout inward the masonry blocks to bond the surfaces of the prism, or to insert synthetic strips between the blocks.

Anand and Ramamurthy [27] analysed two geometric interlocking systems using different ways of the dovetail connection and two different normal concretes with the proportions 1:2:4:0.55 and 1:3:5:0.6 (cement:sand:coarse aggregate:w/c). The first concept was based on blocks with a part coming out as a dovetail (I-shape). The second concept was a channel shape that can also be considered as the negative of the first one. In the next step, wallets were created and evaluated on their axial and eccentric load-bearing capacity as well as on their bending resistance. The latter was subdivided in tension parallel to the bed joint and a tension normal to the bed joint (Fig. 1). Both systems resulted in a high-efficiency factor for the compressive strength (0.62–0.77) as well as for the eccentric-to-axial capacity ratio compared to the conventional masonry. Furthermore, the I-shaped and the channel-shaped concept reached a bending resistance normal to the bed joint comparable to a mortar-bedded prism.

Kohail et al. [29] analysed and compared the behaviour of a conventional wall (conventional block, Fig. 2) to two dry-stacked interlocking masonry blocks systems (i.e. Sparlock system and Azar system, Fig. 2). It was found that the conventional block had the highest compressive strength of 12.10 MPa, while Sparlock and Azar systems achieved the compressive strengths of 6.9 MPa and 8.40 MPa, respectively. Two systems were explored on the stacked system, one using grouted masonry blocks and another using un-grouted ones. The conventional system reached the highest compressive strength for both systems (8.9 and 10.2 MPa).

Chewe et al. [30] analysed the impact of the geometrical imperfections on the load-bearing capacity of a dry-stacked wall, more precisely the height differences and the surface roughness, using numerical and analytical approaches with a comparison against experimental test results from Agaajani [12]. The analysis was performed on single masonry blocks and masonry panels of different heights. The height distribution of the masonry blocks followed a Gaussian law of +/- 2 mm. Chewe et al.

[30] claimed that the height imperfections impact the load-bearing capacity of the wall and distinguished 5 cases of the load percolation on a single masonry block (Fig. 3). This statement was based on the random distribution of blocks with different heights in the wall, which induced a random load percolation system leading to five possible individual loading cases of a masonry block. On each case on top of the masonry block acts a load on the full or the half-length of the block and the percolation of the load is distributed differently for each case on the lower part of the block. A three point loading is unlikely to be generated due to the offset of exactly one half block. Therefore, this load is not included in the 5 cases. Furthermore, they analysed the useful section of a masonry block on a wall. They concluded that the section is statistically reduced related to an increase in the wall height and length. In this paper, a similar occurrence is expected on the wallet based on Miscanthus concrete masonry blocks.

Chewe and Waldmann [31] investigated the improvement of the load-bearing capacity of the masonry blocks with an increase of the useful section by introducing a contact layer on top of each masonry block. The blockwas composed of two face-shells connected by two web faces. The contact layer should lift the height and the roughness imperfections of a block due to its low stiffness [32]. Four contact layers were considered using four distinguished materials with a compressive strength of 5.2–38 MPa and a Young's Modulus of 3–11.5 GPa. A low Young's Modulus has the advantage of alleviating a higher amount of stress peaks but with the detriment of generating significant lateral deformations. Chewe and Waldmann [31] evaluated the load-bearing capacity of these masonry blocks with their respective contact layers on dry-stacked walls of $1000{\times}830$ mm and compared them to a dry-stacked wall with the same dimension and using masonry blocks without any contact layer. During the experimental tests, they have observed that there were three different damages: (1) a crack on the outer face-shell; (2) cracks on the face-shell connection to the web face; and (3) spalling around the bed-joint interfaces. Chewe and Waldmann [31] observed a load-bearing capacity of 4.83 MPa on the wallet using the masonry blocks with a contact layer, which was 32 % higher than the load-bearing capacity of the dry-stacked wall using masonry blocks without a contact layer. In this paper, the use of masonry blocks based on Miscanthus concrete for the wallets is analysed, and it is expected that the impact of the roughness and the height differences will be reduced due to the low Young's Modulus of this material [33].

For a conventional wall with mortared joints, the load-bearing capacity can be determined according to the standard EN 1996-1-1 [34] using different constants, the compressive strength of the mortar and the masonry unit. Chewe and Waldmann [31] expanded the proposed equation from the EN 1996-1-1 to be used on dry-stacked masonry walls by implementing the imperfections of a masonry unit, more precisely the roughness and the height variation. The height was determined by measuring over 100 masonry blocks, and as for Agaajani [12], a
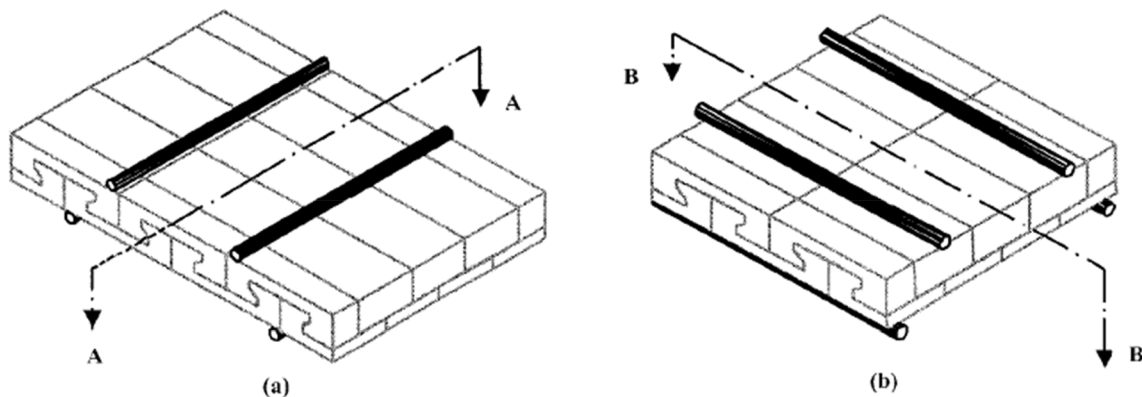

Fig. 1. Bending loading (a) tension parallel to bed joint; (b) tension normal to bed joint ().
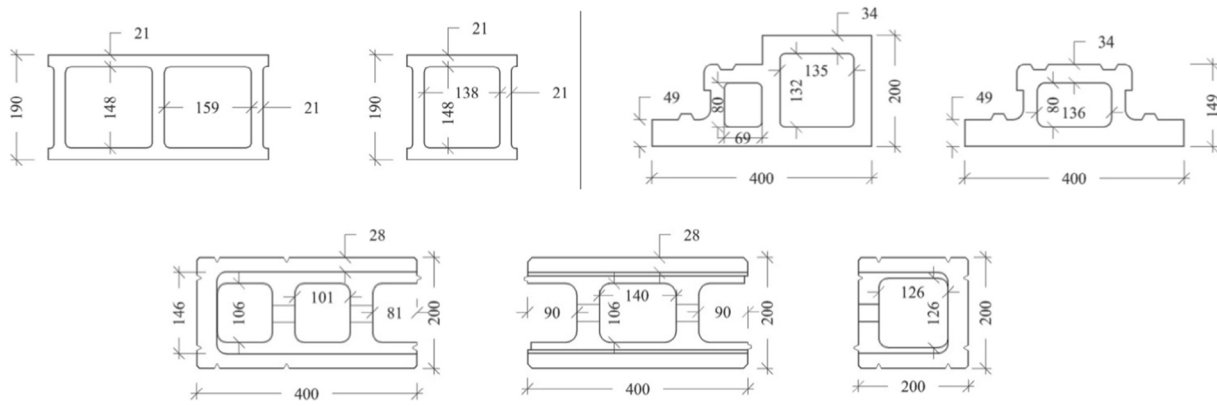adapted from [27]

Fig. 2. Geometry and dimensions of the three analysed blocks, conventional block (left, top), Sparlock system (right, top) and Azar system (middle, bottom) (unit: mm), adapted from Kohail et al. [29]
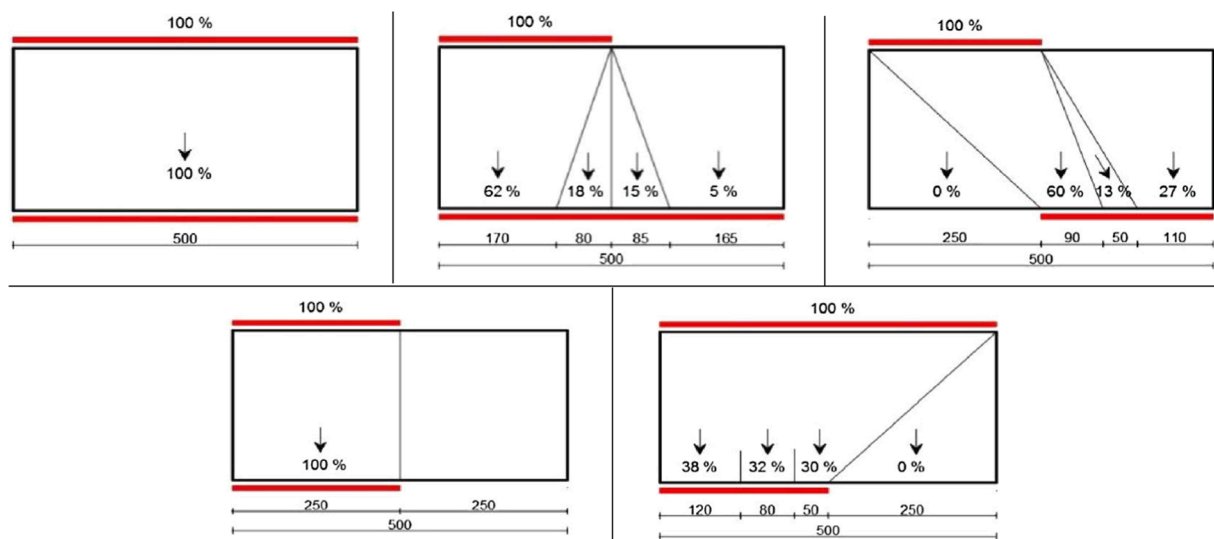

Fig. 3. 5 cases of the load percolation, adapted from Chewe et al. [30]

Gaussian distribution was established with a mean elevation of 200.2 mm and a standard deviation of 1.0 mm. The asperity height of the roughness of the masonry blocks was evaluated by the rate of the actual area in contact. Therefore, Prescale FUJIFILM strips were set on the joints of three stacked masonry blocks. The resulting colour distribution of the strips was analysed by transforming the colour intensity and density in a digital form and by subsequently deducing the actual contact area obtained in the experimental test. For this, an algorithm was created in MATLAB. Chewe and Waldmann [31] determined that a masonry block without contact layer showed a net contact area of 23 %. In contrast, a contact layer on top of the masonry unit increased the contact area. The gain of contact area depends on the material of the contact layer [31,35] and induces an increase in the load-bearing capacity of a dry-stacked masonry wall [36,37]. In this paper, the contact area is determined using a similar technique with the Prescale FUJIFILM.

2. Introduction

The objective of this paper is to investigate the suitability of Miscanthus masonry blocks on dry-stacked walls. Therefore, the mixture composition and the mixture procedure are first studied on a single masonry block and then these findings are applied on wallets. Furthermore, since Chewe and Waldmann [31] stated the roughness and the height differences of the masonry blocks influences the load-bearing

capacity of a wallet, the impact of these imperfections are also analysed for a dry-stacked masonry wallet based on a much more ductile Miscanthus concrete. In addition, a numerical model, suitably validated using the generated experimental data, is developed to study the impact of the roughness and the height imperfections on the load-bearing capacity of the wallet.

3. Materials and experimental and numerical approach

3.1. Materials and mixtures

The Miscanthus concrete mixtures were based on the study performed by Pereira Dias and Waldmann [33]. The constituents of the mixtures were pre-treated MxG fibres, cement (CEM I, 42.5 R), tap water, hydraulic lime (NHL 3.5), calcium chloride ($CaCl_2$) and a superplasticiser (MasterGlenium® ACE 456). In this study, the fibres (length: 1.5–2 cm, diameter: 0.10–0.30 cm, density: 120 kg/m^3) were not priory pre-treated due to their low benefit [33]. Besides the physical and mechanical advantages, it also has the convenience of reducing the whole procedure by one-step and discards the need for a second repository for the treated fibres. The composition of the mixtures (Mix 1, Mix 2, Mix 3 and Mix 4) used in this study are reported in Table 1. The four mixes had an identical amount of Miscanthus and of cement, as well as an identical fibre/cement (F/C) and lime/cement (L/C) ratio. The main difference between the mixes 1–4 is the water/cement (W/C) ratio

Table 1
Composition of the mixtures.

Sample ID	Miscanthus [kg/m^3]	Cement [kg/m^3]	W/C ratio	L/C ratio	W/B ratio	F/C ratio
Mix 1	150	593	0.62	0.55	0.40	0.25
Mix 2	150	593	0.70	0.55	0.45	0.25
Mix 3	150	593	0.80	0.55	0.52	0.25
Mix 4	150	593	0.90	0.55	0.58	0.25

Abbreviations: W/C: Water/Cement ratio; L/C: Lime/Cement ratio; W/B: Water/Binder ratio; F/C: Miscanthus Fibres/Cement ratio.

and the water/binder (W/B) ratio. The amount of the superplasticiser and the CaCl$_2$ were $5.8-5.9 kg/m^3$ and $13.2-13.3 kg/m^3$, respectively.

These materials were used to create three mixture procedures (A, B and C in Table 2). The first step in the preparation of mixtures was to mix two components (Comp.) in dry condition. As given in Table 2, Miscanthus and lime were mixed for mix A, while cement and lime were mixed for mix B and C. After blending for one minute, the water including the dissolved superplasticiser and the CaCl$_2$ was poured into the dry mixture. Depending on the mixture, half or full amount of water was added and blended for 2–2.5 min at this step. After that, the remaining component, i.e. cement for mix A and Miscanthus for mix B and C, was added. The mixtures (A and C) were then blended for 1 min and the remaining water was poured into the blender. Finally, the mixtures were blended for another 3–3.5 min.

After a total blending time of 7–7.5 min, the final mixtures were used to prepare test prisms of 16x4x4cm and masonry blocks of 40x20x10cm. The prisms were moulded in a precision three-gang mould (left in Fig. 4) according to the EN 196. The masonry blocks were created in self-made wooden formworks (middle and right in Fig. 4). Dependent on the analysis, one mix was performed to fill prisms and masonry blocks. In this case, the masonry blocks were always produced before the prisms due to their higher volume and to avoid a more substantial settlement of the fresh concrete, which would induce bleeding of the Miscanthus concrete. Independent from the shape of the specimen, the moulding procedure was the same. The mould was first half-filled, hand-compacted and vibrated for 5 s. Next, the remaining part of the mould was filled until the top, and as in the previous step; it was hand-compacted and shook for 5 s. Finally, if needed, more material was poured inside, and the mould was covered with a wooden plate to enclose the surface in contact with the ambient.

After one day of curing in laboratory conditions, the specimens were removed from the moulds, weighed and wrapped with cellophane to avoid an excess of water evaporation. After 13 days of curing, the translucent was removed and the specimens were stored under ambient conditions until reaching a total curing time of 14 or 28 days.

3.2. Experimental approach

The suitability of Miscanthus concrete on masonry blocks and wallets was analysed in 5 steps (Trial 1–5 in Table 3). According to Pereira Dias and Waldmann [33], the W/C ratio has a high impact on the achieved load-bearing capacity of prisms and cubes. Therefore, the first study (Trial 1) consisted of analysing the impact of the W/C ratio (varying the water amount) on the compressive strength using the mixing procedure A (Table 2) on the mixtures Mix 2, Mix 3 and Mix 4 (Table 1). For

Trial 1, six prisms and two masonry blocks were produced per mixture. The presented compressive strength of the prisms was averaged out of three prisms per variation according to the standard DIN EN 197-1 [38]. Each masonry block of Trial 1 was produced by filling the mould from the top surface (middle Fig. 4). Due to the cement settlement during casting, the filling procedure for the masonry blocks from the following trials was adapted and the mould in Fig. 4 (left) was used. Tables 4 and 5

A critical factor in achieving a homogenous masonry block is a uniform distribution of the mix components. Therefore, the mixing procedure's impact (A, B and C in Table 2) on the compressive strength was analysed using Mix 2 in another test (Trail 2). For Trail 2, six prisms were produced using each mix. It is assumed that a combination of Trial 1 and 2 would assess the achieved load-bearing capacity. Accordingly, the subsequent analysis (Trial 3) comprised a variation of the water amount (similar to Trial 1) but using the mixing procedure B on Mix 1 and 2 to set up six prisms and six masonry blocks per mix. Furthermore, it is known that the rheological properties of ordinary concrete are impacted by vibration [39]. Therefore, in addition to the stated analysis of Trial 1, 2 and 3, the impact of vibration on the compressive strength was evaluated by comparing the vibrated specimens with the non-vibrated ones. Trial 4 was divided into two parts; both were based on Mix 2 and the mixing procedure B. It is expected that the curing time affects the load-bearing capacity. Thus, in the first part, the compressive strength of masonry blocks and prisms after a curing time of 28 days was analysed. Besides, the contact surface of the masonry blocks was simultaneously evaluated. The peaks of the roughness are crushed with an increasing load. Therefore, the second part consisted of putting a stepwise load (loading and unloading) on a masonry block cured for 14 days, and analysing the contact surface at each load-step of 1 MPa as well as the final load-bearing capacity. Finally, to analyse the suitability of the masonry blocks for use on a dry-stacked wallet, 18 masonry blocks were created in Trial 5, which were used at the age of more than 90 days to create 3 dry-stacked wallets (Wallet 1–3).

Each wallet had a height of 3 and a length of 2 masonry blocks (60x80cm) (Fig. 5). The lower and the upper row (R1 + R3) consisted of two full masonry blocks, and the middle row (R2) is composed of one entire block and two half-blocks. The masonry blocks were staggered above each other without any mortar in the bed joints (J1 + J2). For a better analysis of the experiment, the vertical deformation of the bed joints and each masonry block was measured. The deformation between the rows is measured using the sensors on the front (front in Fig. 5). The transducers positioned on R1, R2 are averaged as D_R1 and the captors measuring the vertical deformation from R2 and R3 are averaged as D_R2. Furthermore, the deformation in the third row (D_R3) is calculated by deducting D_R1 and D_R2 from the total deformation of the wallet. The sensors on the back measured the vertical deformation in the bed joints (D_J1 and D_J2). Since the slenderness ratio of the walls is only 4.5 due to the small wall height of 60 cm and a width of 10 cm, the out-of-plane deformation is assumed to be negligible and is therefore not measured in the framework of the presented experiments.

To apply a uniform compressive loading on the masonry blocks 4 and 5 (Fig. 5) a steel beam (HEA180 – S235) has been used and fixed to the cylindrical hydraulic press with a maximum loading capacity of 1 MN. The vertical displacement of the steel beam was measured using two transducers on top of this steel beam (D-Tot-L and D-Tot-R in Fig. 5).

The aim of Wallet 1 was to measure the load-bearing capacity of the masonry blocks based on Miscanthus concrete. Therefore, no contact

Table 2
Mixing procedure.

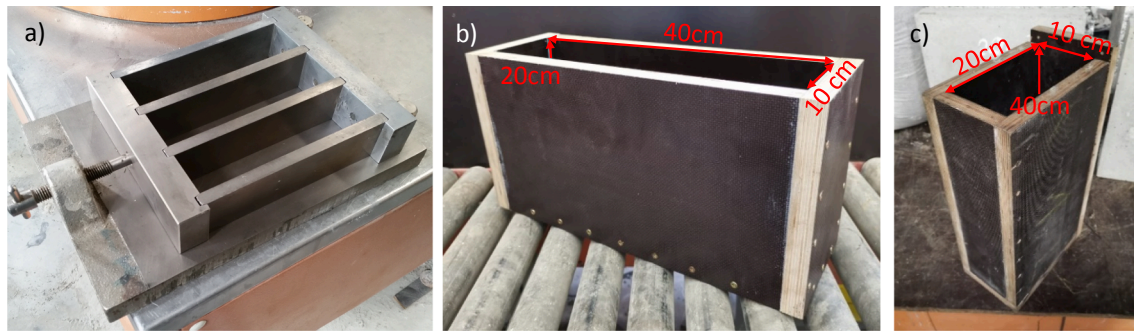| Name	Comp.	Mix. time	Comp.	Mix. time	Comp.	Mix. time	Comp.	Mix. time	Total time
A	Miscanthus + Lime	1 min	Half of the water amount*	2 min	Cement	1 min	Remaining water	3.5 min	7.5 min
B	Cement + Lime	1 min	Complete water amount*	2.5 min	Miscanthus	3.5 min	–	–	7 min
C	Cement + Lime	1 min	Half of the water amount*	2 min	Miscanthus	1 min	Remaining water	3 min	7 min

* Including ACE 456 and CaCl$_2$.

Fig. 4. Mould and dimensions of the samples: a) prisms, b) and c) masonry blocks.

Table 3
Experimental trials.

Trial	Used Mixes	Mixing procedure	Vibration analysis	Contact analysis	Curing Time [d]	Created specimens per mix
Trial 1	Mix 2	A	Yes	Yes	14	6 Prisms
	Mix 3					2 Masonry blocks
	Mix 4					
Trial 2	Mix 2	A	Yes	–	14	6 Prisms
		B				
		C				
Trial 3	Mix 1	B	Yes	Yes	14	6 Prisms
	Mix 2					6 Masonry blocks
Trial 4	Mix 2	B	–	Yes	28	3 Prisms
						3 Masonry blocks
				Stepwise	14	3 Masonry blocks
Trial 5	Mix 2	B	–	–	90	18 Masonry blocks

analysis was performed on Wallet 1 and no transducers were applied on the back part of the wallet and on top of the steel beam. The load was continuously applied (at a rate of 2 mm/min), contrarily to Wallet 2 and 3, where the application of the pressure was controlled to form a hysteresis curve. In addition, a contact analysis was performed on J1 and J2 of Wallet 2 and 3.

All the contact analysis previously mentioned were performed using strips of a two-sheet type of Prescale FUJIFILM (left in Fig. 6), which is composed of two films (A + C) put above each other with the colour layers together. Film A has a red-colour-forming layer with microcapsules on one side and Film C has a layer, which develops a colour using the absorbed microcapsules that break due to a pressure application. The breakage depends on the measurable pressure range. In this study, since the contact on a masonry block was analysed at different loads, the pressure varied from 0.5 to 2.5 MPa (Prescale Super Low Pressure (LLW)). Afterwards, depending on the density of the red colour (dark to light red) (right in Fig. 6), the pressure can be measured using different techniques. Here, the FUJIFILM strips were scanned using a conventional scanner and the colour of the resulting images were converted to grayscale.

Finally, a script was created using MATLAB to analyse each pixel's colour and extracts the grayscaled colour number. This last was compared to a range based on the colour-density (right in Fig. 6), which was also grayscaled before. Each field can be associated with the applied pressure using the diagram in the instruction manual of the Prescale LLW [40], which associates the force to the colour density.

Table 4
Results for Trial 1 of the density, compressive strength and the relative difference between the vibrated and the non-vibrated mixture.

The shape of samples	Mixture	Density [kg/m^3]*			Load-bearing capacity [MPa]*		
		vibrated	Not vibrated	Rel. difference [%]	vibrated	Not vibrated	Rel. difference [%]
Prisms	Mix 2	884.1 (16.3)	705.8 (4.6)	− 20.2	3.30 (0.08)	1.32 (0.15)	− 60.1
	Mix 3	1025.5 (106.3)	1008.4 (26.1)	− 1.7	4.64 (1.27)	2.59 (0.26)	− 44.2
	Mix 4	1008.4 (83.6)	949.0 (139.9)	− 5.9	3.44 (0.75)	3.23 (0.99)	− 6.0
Masonry blocks	Mix 2	1063.5	934.1	− 12.2	1.46	0.63	− 57.3
	Mix 3	914.6	1096.8	+ 19.9	1.15	0.99	− 13.9
	Mix 4	1096.8	1144.2	+ 4.3	1.60	1.79	+ 11.9

* Values in brackets represent the standard deviation.

Table 5
Results for Trial 2 of the density, compressive strength and the relative difference between the vibrated and the non-vibrated mixture.

Prisms	Density [kg/m^3]*			Load-bearing capacity [MPa]*		
Mix Procedure	vibrated	Not vibrated	Rel. difference [%]	vibrated	Not vibrated	Rel. difference [%]
A	1118.2 (16.2)	998.4 (9.3)	− 10.7	4.32 (0.62)	3.11 (0.25)	− 28.0
B	1089.2 (13.1)	1031.5 (35.7)	− 5.3	5.06 (0.46)	3.65 (0.80)	− 27.8
C	973.0 (22.1)	841.0 (23.4)	− 13.6	3.17 (0.29)	1.54 (0.20)	− 51.5

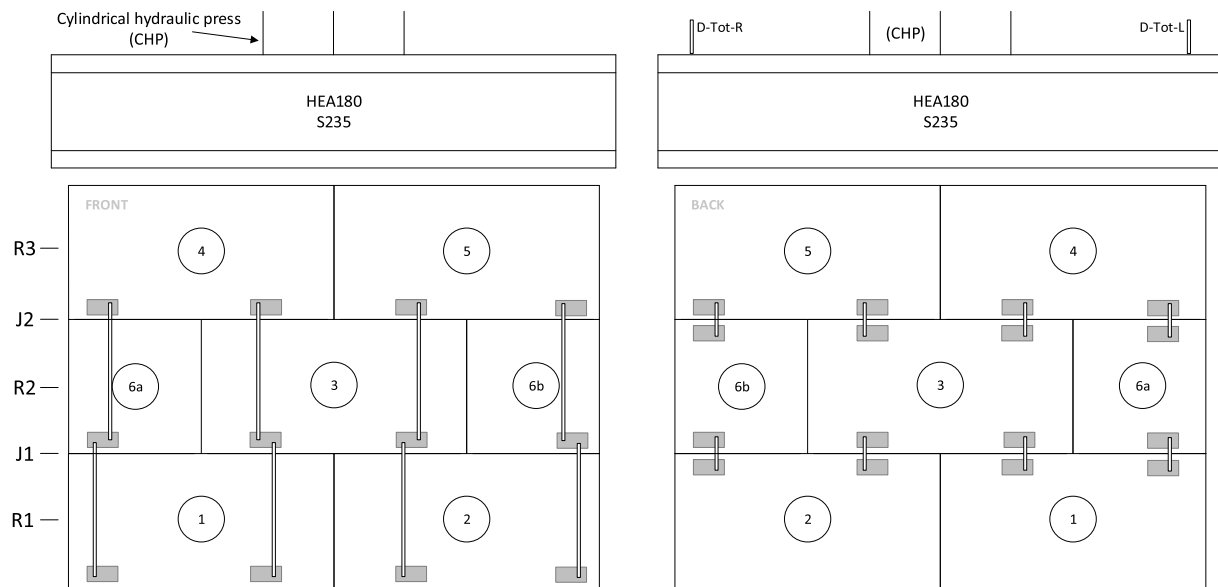* Values in brackets represent the standard deviation.

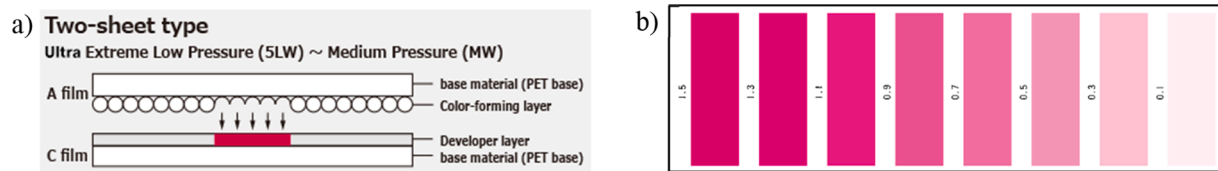**Fig. 5.** Position of the masonry blocks and the transducers.

Fig. 6. a) Features of the used Prescale FUJIFILM and b) the densities of the red colour (no unit) [40].(For interpretation of the references to colour in this figure legend, the reader is referred to the web version of this article.)

3.3. Analysis of the height imperfections of masonry blocks

During the production process of conventional masonry blocks, the height of the masonry blocks is not constant and follows a Gaussian distribution [12]. This occurrence is also expected on the masonry blocks based on Miscanthus concrete. Therefore, the masonry blocks were dimensioned and categorised according to their production mould (middle and right Fig. 4) before being tested.

4. Results and discussion

In the following sections, the load-bearing capacity and the roughness are analysed for each trial presented in Table 3. In addition, the height imperfections are studied by measuring the height of the masonry blocks and creating a normal distribution according to the data. A numerical parameter study is performed on a validated model for one masonry block. Then, a numerical wall is modelled using the validated parameters from the single masonry block and the impact of the height differences as well as the impact of the dimensions of the wall on the load-bearing capacity are analysed.

4.1. Load-bearing capacity

4.1.1. W/C ratio variation

The achieved load-bearing capacity of the prisms, and masonry blocks from Trial 1 as well as their densities are shown in Table 6. The presented results of the prisms are a mean value out of three measurements, while each result of the masonry blocks is based on one test. The vibrated mixtures developed a denser structure due to reduced free water in the mix, which compromises the bond fibre matrix [41–43]. As the vibration ends up expelling the voids from the sample, the matrix is better compacted and consequently, presents a higher density [44]. Vibrating the prisms relates to an increase of 2–21% of the density compared to the non-vibrated ones. It is noticeable that the higher the W/C ratio, the less the vibration action has an impact on the final density.

A similar observation is done for the achieved compressive strength, where the practice of not vibrating the prisms reduced the achieved strength by 6–60%. If these results are compared to literature, it becomes evident that a higher compressive strength could be achieved when the W/B ratio is low. As stated in Refs. [45,46], W/B ratio between

Table 6
Results for Trial 3 of the density, compressive strength and the relative difference between the vibrated and the non-vibrated mixture.

The shape of samples	Mixture	Density [kg/m³]*			Load-bearing capacity [MPa]*		
		vibrated	Not vibrated	Rel. difference [%]	vibrated	Not vibrated	Rel. difference [%]
Prisms	Mix 1	880.6 (16.8)	770.0 (21.9)	− 12.6	1.83 (0.19)	1.14 (0.44)	− 37.5
	Mix 2	1040.7 (25.6)	902.4 (46.6)	− 13.3	3.78 (0.49)	2.24 (0.45)	− 40.8
Masonry Blocks	Mix 1	1006.0 (23.8)	875.1 (42.1)	− 13.0	1.84 (0.27)	0.64 (0.26)	− 65.1
	Mix 2	1154.3 (25.7)	1078.3 (34.9)	− 6.6	3.44 (0.45)	2.35 (0.55)	− 31.7

* Values in brackets represent the standard deviation.

1.16 and 1.59 led to densities between 291–500 kg/m^3 and compressive strengths from 0.18 to 0.85 MPa. The highest compressive strength was achieved by Arnaud et al. [46] with a W/B of 1.30 and a density of 500 kg/m^3. However, in this trial, similar to the study performed by Pereira Dias and Waldmann [33], the prisms with a W/C ratio of 0.8 (Mix 3, W/B = 0.52) and 0.9 (Mix 4, W/B = 0.58) reached a higher compressive strength than Mix 2 (W/C = 0.7 and W/B = 0.45).

The prisms with a higher W/C-ratio (i.e. Mix 4) are less homogeneous in their structure, forming a hardened material at their base due to the high water amount. The latter induces a division of the specimen. Due to the seeping of water and cement, the lower part of the specimen was more rigid than the upper part, where a large amount of Miscanthus was visible. At the time of compaction, the upper part of the prism was more deformable and fragile due to a grouping of grains.

The stress–strain distribution achieved by the prisms from Trial 1 are shown in Fig. 8 (left). Each test is averaged from 3 specimens with a standard deviation varying from 0.08 to 1.27 MPa (Fig. 8 right). The behaviour of the prisms from Mix 2 (Fig. 7) can be defined as ductile elastoplastic, as large deformations are developed before maximum strength is reached (Fig. 8 (left)). This behaviour is not the case for Mix 4 and the vibrated Mix 3, which comes to its full capacity more quickly by the less ductile material formed at the base of the prism.

The Miscanthus-to-binder ratio tends to exhibit a higher degree of ductility, as reported in the literature [47–49], where fibres are characterised by a high degree of porosity, resulting in a high deformation capacity. As can be seen in Fig. 8, the W/B ratio has a strong influence on the deformation capacity and prism resistance, which is clearly visible on the not vibrated mixtures. As the W/B ratio increases, the deformability rate decreases. This statement can be well observed for the mixtures where the vibration during the filling procedure was omitted.

The masonry blocks (Fig. 9) based on the same mixture composition as the prisms delivered a different behaviour, which indicates a shape dependency of each mixture for the load-bearing capacity, as claimed by Pereira Dias and Waldmann [33] and Pavía [50]. The ultimate load showed to be lower for all the masonry blocks compared to the prisms, even if in most cases the density of the block was higher than the one of the prisms. As for the prisms, the impact of vibration during casting on the load-bearing capacity was reduced with an increase of the W/C ratio (Table 6). Except for the masonry blocks based on the mixture with a W/C ratio of 0.9 (Mix 4), which achieved a load-bearing capacity of 11.9 % higher by omitting the vibration.

4.1.2. Analysis of the mixing procedure

Next, the impact of the mixing procedure is analysed (Trial 2). The achieved load-bearing capacity and density by the prisms are presented in Table 7. It is noticeable that the prisms based on the mixing procedure C achieved the lowest density. In addition, these same prisms showed to have the highest reduction in density (13.6 %) due to an absence of vibration. For this mixing procedure, it can also be seen that the smallest compressive strength was obtained in both categories: for the vibrated specimens 3.17 MPa and for the not vibrated sprecimens 1.54 MPa.

The prisms based on the mixing procedure A achieved the highest density (1118.2 kg/m^3) and reached a compressive strength of 4.32 MPa. These results were higher than the ones from Trial 1 (884 kg/m^3

and 3.40 MPa), despite using the same components and conditions. The occurrence is due to a difference during the manual filling procedure of the mould, where more material had to be squeezed to fill the mould up to the top, which resulted in a higher density.

The vibrated prisms based on the mixing procedure B achieved the highest load-bearing capacity (5.06 MPa). This method also reached the lowest relative difference of the density (5.3 %) between the vibrated and the non-vibrated mixture. The main reason for this procedure being the most promising was the fact that cement and lime were first mixed with the full amount of water to generate a liquid paste and the Miscanthus was poured after 3.5 min of blending. This technique provides the binders to use the water needed for their chemical reactions before the Miscanthus fibres start to absorb the water. After blending the binders with water, Miscanthus is poured and is enveloped with the liquid paste. Then, it only starts to absorb the excess water of this paste due to its porous structure and high absorption capability. For this reason, the Miscanthus fibres, which only had access to the remaining water and which was not used by the binder, made the samples develop a better mechanical behaviour.

4.1.3. Combination of mixing procedure and W/C ratio

Trial 3 consisted of using the mixing procedure, which previously gave the highest compressive strength on Mix 2 and compare it to Mix 1, which has a lower W/C ratio. The density and the compressive strength of Mix 1 (Table 8) showed to be lower than Mix 2 independent from the shape of the analysed specimen. The reduction of the W/C ratio from 0.7 to 0.62 causes a reduction of the density of the prisms by 15 % and their compressive strength is reduced by 49–51 %.

A similar behaviour could be observed on the masonry blocks, a reduction of the W/C ratio induced a decrease of the density by 7–13 %. The compressive resistance was diminished by 46 % for the vibrated specimens and by 73 % for the non-vibrated ones. Furthermore, the impact of the vibration on Mix 1 was 1.7 times higher on the masonry blocks than on the prisms. Therefore, at this stage, two aspects could be deduced.

The first observation, a decrease of the W/C ratio induces a lack of water in the mixture and consequently achieves a lower resistance. The second point is regarding the vibration. Independent from the mixing procedures, analysing the impact of the vibration on the mixes from Trial 1 and Trial 3, it can be stated that if the W/C ratio decreases, a vibration during moulding affects more the compressive strength of the Miscanthus concrete than increasing the W/C ratio. A reason for this is that an increased W/C ratio, as Mix 4 in Trial 1, in combination with vibration can cause segregation of Miscanthus from the binders.

4.1.4. Analysis of curing time of 28d and stepwise loading

The analysis of the specimens cured for 28-days is essential to verify the development of the material properties, helping to characterise the mechanical behaviour of Miscanthus-based blocks. Therefore, Mix 2 with the mixing procedure B was used, as it showed the most favourable results considering the compressive strength (Table 6, Table 7 and Table 8). In this section, the prisms cured during 28 days are analysed, followed by a similar analysis on the masonry blocks and finalising with a discussion about the achieved load-bearing capacity by loading and unloading a masonry block cured for 14 days.

4.1.4.1. Analysis of the specimens cured for 28 days.
The prisms showed a difference in the compressive strength of 3 % between a curing time of 14 and 28d (Table 9). This modest difference can be explained by the low density of the prisms at 28d (922.1 kg/m^3), which is a reduction of 11.4 % related to the density at 14d (1040.1 kg/m^3). The reduction of the density can be explained by the higher curing time, which implies a higher amount of evaporated water in the matrix.

As can be seen in Table 9, the masonry blocks cured for 28d reached a compressive strength of 5.42 MPa, which is an increase of 57.5 %

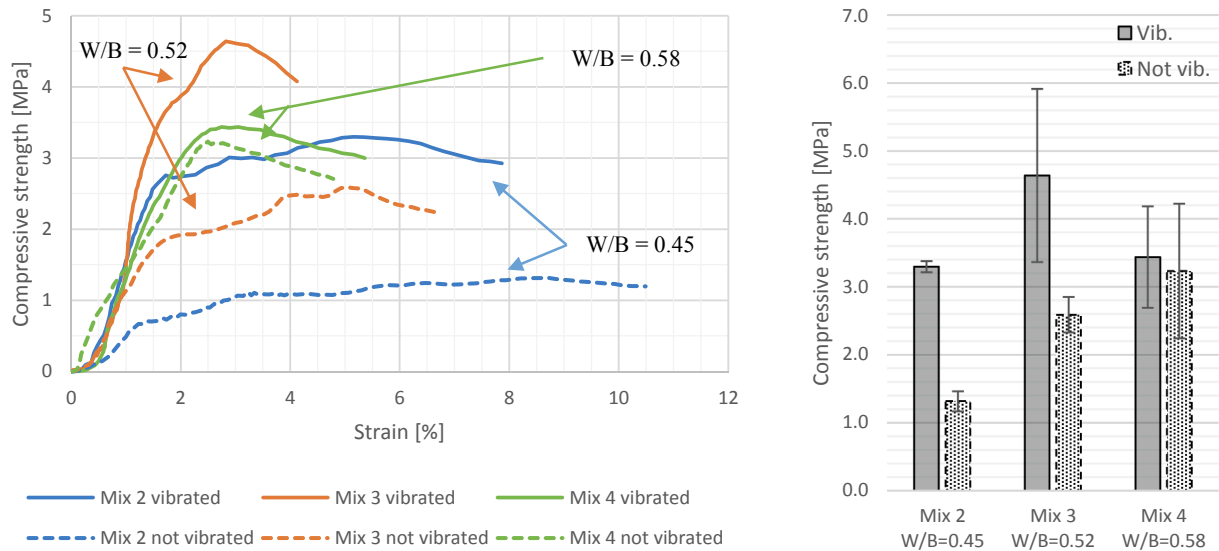**Fig. 7.** Mix 2 vibrated (left) and not vibrated (right).

Fig. 8. (Left) Stress-strain curves of the prims at 14 days from Trial 1 and (right) achieved compressive strength in [MPa] and standard deviation of 3 specimens per test.
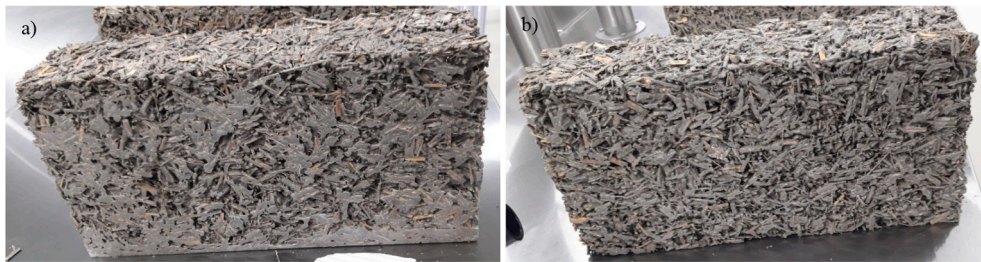

Fig. 9. a) Vibratedand b) non-vibrated masonry blocks based on Mix 2.

Table 7
Results for Trial 4 of the density and the compressive strength for 14 and 28 days.

The shape of samples	Curing time [d]	Density [kg/m³]*	Load-bearing capacity [MPa]*
Prisms	14	1040.7 (25.6)	3.78 (0.49)
	28	921.7 (4.1)	3.81 (0.36)
Masonry Blocks	14	1154.0 (25.7)	3.44 (0.45)
	28	1082.1 (6.2)	5.42 (0.23)
Masonry Blocks**	14	1191.6 (9.3)	4.75 (0.21)

** stepwise load.
* values in brackets represent the standard deviation.

Table 8
Results for Trial 5 of the density, the load-bearing capacity, the deformation at and the plastic deformation after reaching the load-bearing capacity.

The shape of samples	Density [kg/m³]	Load-bearing capacity (LBC) [MPa]	Strain at LBC [%]	Plastic strain [%]
Wallet 1	1121.6	4.84	1.21	0.50
Wallet 2	1146.1	5.65	1.19	0.49
Wallet 3	1125.6	5.56	1.16	0.46

compared to a curing time of 14d (3.44 MPa from Trial 3). The density decreased by 6.3 % over a time of 14d. This huge difference in the compressive strength is due to the water evaporation in the specimen that takes longer for a masonry block (40x20x10 cm) than for a prism (16x4x4 cm). Due to the high volume of the masonry block, time to achieve its final compressive strength is increased. Hence, it can be

Table 9
Plastic strain [%] after each load-step.

Plastic strain (at the end of each load step) [%]	Load 1 (1 MPa)	Load 2 (2 MPa)	Load 3 (3 MPa)	Load 4 (4 MPa)	Final Load (at LBC)
Wallet 2	0.11	0.17	0.19	0.24	0.49
Wallet 3	0.06	0.09	0.17	0.24	0.46

concluded that a specimen with a high volume based on Miscanthus concrete is more sensitive to the curing time than one with a lower volume. Thus, it is clear that the mechanical behaviour is affected by the shape and size of the samples [50].

In comparison to the presented results, Juárez C. et al. [51] analysed the load-bearing capacity of hollow concrete masonry blocks containing a natural fibre from Mexico, the agave lechuguilla. The highest load-bearing capacity of 2.15 MPa, which is about 60% lower than the developed masonry blocks with a fibre/cement content of 0.25 in this study, was achieved with a fibres/cement ratio of 0.05 and a density of fine and coarse aggregates of 1822 kg/m³. Awwad et al. [52] implemented hemp fibres into a full concrete masonry block with 2210 kg/m³ of fine and coarse aggregates and a fibres/cement ratio of 0.02 was used. The hemp masonry blocks achieved a compressive strength of 6.1 MPa, which is 12.5 % higher than the masonry blocks presented in this paper, but with the disadvantage of having 12.5 times lower fibre/cement ratio. A load-bearing capacity of 20.8 MPa of a hollow concrete masonry block used for dry-stacked walls was measured by Chewe and Waldmann [35]. Bernat et al. [53] measured compressive strength of 27.93 MPa on a solid-clay brick. Both non-fibrous masonry blocks resulted in 3.8–5.15 times higher load-bearing capacity than the masonry block

cured for 28 days based on Miscanthus and presented in Table 9.

4.1.4.2. Impact of a gradual loading. The second part of Trial 4 consisted of analysing the behaviour of masonry blocks with gradually loading. This procedure was performed by loading and unloading the masonry blocks in steps of 40 kN. On average, the masonry blocks with a density of 1191.6 kg/m^3 achieved a compressive strength of 4.75 MPa after a curing time of 14d (Table 9). The masonry blocks, which were subjected to a gradual loading, achieved in average a 38 % higher compressive strength compared to masonry blocks that were continuous loaded (3.44 MPa). This can be explained by the known effect, represented by the coefficient α_{cc} from normal concrete, which reduces the characteristic strength by 0–20 % [54]. This reduction factor is, among other reasons, applied due to effects resulting from the duration the load is applied. Since a continuous load implies a shorter time test, the load-bearing capacity of a short time test is always reduced compared to a long time test due to creeping effects. The coefficient α_{cc} is between 0.8 and 1.0 for a normal concrete [54]. The behaviour of a concrete based on Miscanthus aggregates is different in several aspects and therefore, a lower reduction factor of $\alpha_{cc} = 0.62$ has been measured. This value is lower than the minimum value imposed by the standard because the masonry blocks had only a curing time of 14 d.

4.1.5. Analysis on wallets

The experimental wallets (Fig. 10) created with the Miscanthus-based masonry blocks served to analyse the mechanical behaviour of the material by applying a compressive strength until reaching the load-bearing capacity of the system (Trial 5). Even after the structure reached its ultimate load (Table 8), the masonry showed almost no visual cracks, loss of stability or inclination (Fig. 11, a). Furthermore, the structure remained stable and functional at load-bearing capacity.

Wallet 1 had a strain of 1.21 % at its load-bearing capacity of 4.84 MPa (Fig. 12) and after unloading the wallet, a plastic strain of 0.50 % could be measured. Due to the heterogeneous surface of the wallets, the analysis of crack development was difficult. Only three places with cracks could visually be investigated on the wallet after reaching its load-bearing capacity and being unloaded (Fig. 11a)). These cracks are a consequence of the impact of the geometrical imperfections such as the roughness of the block surface and height differences between the masonry blocks, which lead to local stress concentration as observed by Chewe et al. [31] on conventional masonry blocks in a dry-stacked wall. The local stress concentration due to the height imperfections of the Miscanthus masonry blocks induced an irregular load percolation between each course which leads to the formation of cracks.

Next, the masonry was fully reloaded (post-load) to analyse a compromised failure. At a strain of 4.78 % (Fig. 12), the masonry lost its

stability and the crack pattern, as well as the damage, was visible (Fig. 11b). Nevertheless, due to the fibrous Miscanthus concrete, the wallet behaved ductile during the whole loading and post-loading process.

The stress-strain distribution presented in Fig. 12 shows that no sudden failure occurs on the wallet based on Miscanthus concrete even after reaching its load-bearing capacity and overloading (post-load) the system. The masonry showed a very ductile behaviour in overload collapse situations, with a strain at the load-bearing capacity of 1.16 % to 1.21 %. The ductility of the wall here refers to its ability to deform without significant loss in strength. According to Cohn and Bartlett [55], a ductility coefficient can be calculated using the strain on the post-peak side at 85 % of the load-bearing capacity and the strain of the first yield behaviour of the specimen (Fig. 13). The ductility coefficient of Wallet 1 is 1.47, which is identical to the ductility coefficient of 1.45 presented by Dong [56] for a wall based on recycled concrete and higher than the ductility coefficient (0.91–1.23) of a wall based on lightweight concrete masonry blocks analysed by Lourenço et al. [57]. In general, it can be stated that the higher this coefficient, the higher the plastic deformation.

A cyclic load was applied on wallets 2 and 3 until they reached their load-bearing capacity. The pressure was with every loading step increased by 1 MPa (±80 kN). Fig. 14 shows the hysteric behaviour that occurred on wallet 2 and a detailed view of the stress-strain distribution of wallet 2 until reaching its load-bearing capacity. A clear elastic behaviour is visible after unloading of each load-step showing the ductile behaviour of this material. However, when the pressure is removed, the masonry keeps a plastic deformation, which is increased at each loading step (Table 9). Determined by the phase difference in a given cycle, the applied force tension curve and the displacement curve scheme a hysteresis loop [59].

According to the results presented in Table 8, the wallets submitted to a cyclic loading, achieved a 15–17 % higher load-bearing capacity than Wallet 1, which was continuously loaded. The reason for this occurrence is similar to the one presented on the test of a single masonry block (section 3.1.4.2), where an α_{cc} value of 0.62 was discussed. In the case of the test on the wallets, the α_{cc} value amounts to 0.83–0.85, which is higher than the α_{cc} analysed on the compression test of a single masonry block ($\alpha_{cc} = 0.62$). This difference is related to the longer curing time (90 days) of the masonry blocks used in the wallets. Furthermore, the value for this wall is in the range presented in the standard (0.8–1.0), which validates the presented relation.

The behaviour of all three tests followed the same initial pattern. Even when the samples reached their load-bearing capacity, almost no cracks were visible on the masonry. The fracture lines on the wallet could only be visualised during post-failure loading where a very ductile behaviour of the wallet can be observed, which is advantageous concerning safety aspects. This ductile behaviour is not the case for a dry-stacked wall using conventional masonry blocks based on normal concrete, which is usually less flexible and more rigid [35].

Next, the deformation of each row at ultimate load (D_R1, D_R2 and D_R3), which includes a small part of the deformation of the adjacent blocks, as well as the deformation of the horizontal bed joints (D_J1 and D_J2) are analysed to determine in which row the highest deformation of the masonry blocks occurs (Fig. 15). Except for Wallet 1, the deformation was the highest on the top row (D_R3) and the lowest on the bottom row (D_R1). In a dry-stacked masonry wall, the height differences have a high impact on the behaviour and the load-bearing capacity of the wall [30]. The reason for the deformation of D_R1 being the highest for Wallet 1 is due to the height differences in one masonry block of the bottom row.

The height of the masonry blocks casted with the formwork from Fig. 4 (right) followed a normal Gaussian distribution (Fig. 19) with a standard deviation of $\mu = 0.285$ mm. The load-bearing behaviour of Wallet 2 and 3, which were loaded differently from Wallet 1, was less impacted by the roughness and the height differences of the masonry blocks.
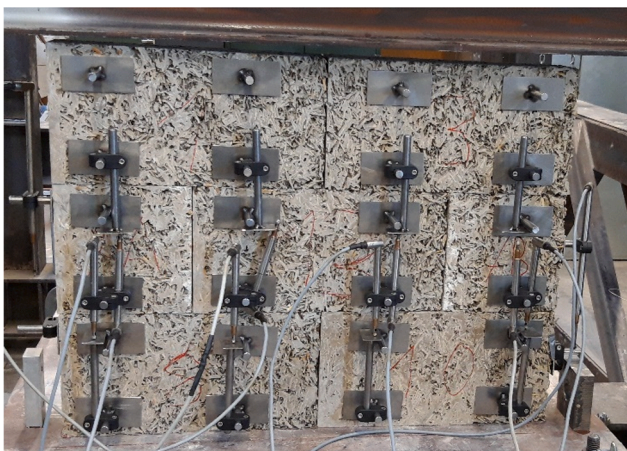

Fig. 10. Test setup in the front part of Wallet 1.

Fig. 11. a) Cracks in Wallet 1 at maximum load capacity; b) Cracks in Wallet 1 after application of the load beyond its maximum capacity (post-load).
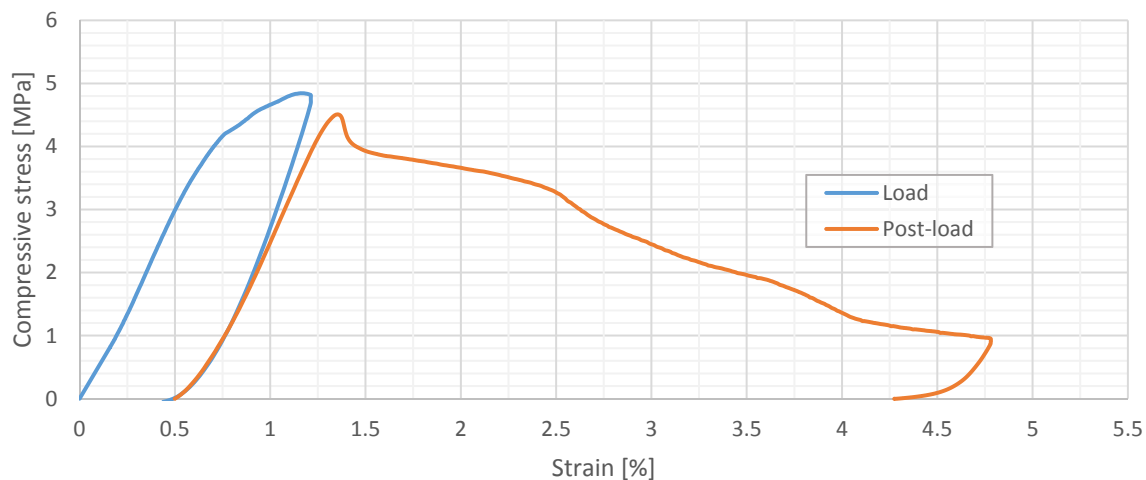

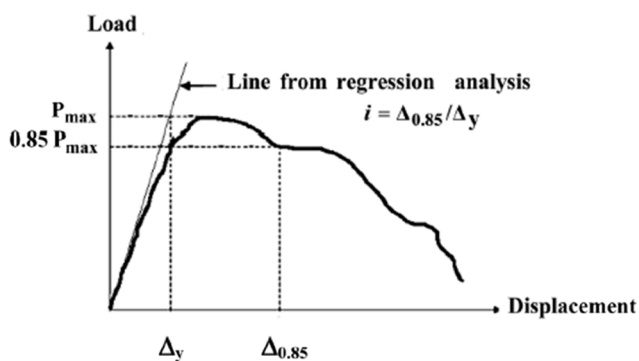**Fig. 12.** Stress-strain curve in the load phase and post-load phase of Wallet 1.

Fig. 13. Definition of displacement-ductility ratio according to Cohn and Bartlett [55] (adapted from Rakhshanimehr et al. [58]).

In this paper, only vertical in-plane loading has been analysed. However, another very important analysis which has to be mentioned is the application of an in-plane shear force or an out-of-plane load. The application of a shear force on a wall comes always with a low vertical compressive load due to self-weight [60]. In the case of a wall based on Miscanthus masonry blocks, the vertical load due to self-weight is relatively low due to their low density compared to conventional masonry blocks. Furthermore, due to the adoption of a dry-stacked system, only the geometrical imperfections and the friction between the rectangular Miscanthus masonry blocks are acting against shear. Therefore, it can be assumed that the presented wallet would have a lower shear resistance compared to dry-stacked walls using conventional masonry blocks. Due to Miscanthus fibres in the masonry blocks, the out-of-plane flexural strength of the presented system can be assumed to be higher than the one of conventional walls. It is clear that the fibres allowed a greater ductility of the system. As stated by Hamoush et al. [61] these occurrences allow the walls to have a greater energy absorption.

4.2. Analysis of the roughness

During the compressive strength test, the contact area of the top and the bottom surface of the masonry blocks was recorded using FUJIFILM strips. In the following sections, the contact area achieved by each trial will be analysed.

4.2.1. W/C ratio variation

The FUJIFILM layers were withdrawn from the upper and the lower surface of the masonry blocks after reaching their load-bearing capacity. The averaged results, based on the top and the bottom surface, showed clearly that the mixtures with a higher W/C ratio (Mix 4) induced a higher contact surface (Fig. 16). This increment is larger if the vibration of the mixture is omitted during casting. Mix 2 showed to be more dependent on the vibration to reach a higher contact area than the other varieties.

Independent from the analysed specimen, the top surface showed to be more even than the bottom surface. This last fact is due to the filling procedure (middle Fig. 4).
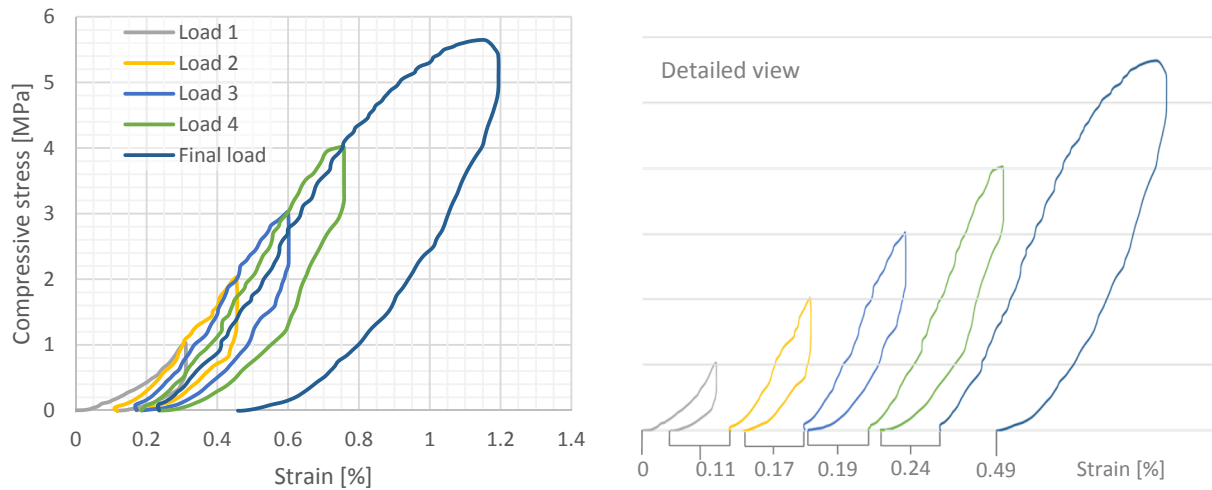
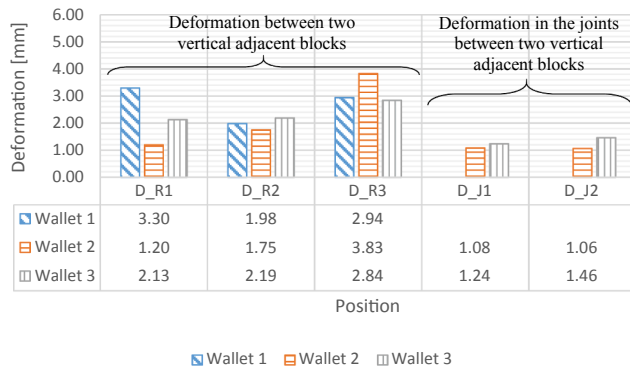**Fig. 14.** Stress-strain curve during the load phase for Wallet 2 as well as a detailed view of the 5 loading steps.

Fig. 15. Deformation [mm] of the masonry blocks in each row measured on the three wallets.

4.2.2. Combination of mixing procedure and W/C ratio

The masonry blocks from Trial 3 were established using the second filling technique and so the loaded surfaces were casted against the framework (right Fig. 4). Due to this alteration, the contact area of Mix 2 from Trial 3 (Table 10) is higher than the contact area from the mixture Ref in Trial 1 (Fig. 16). Furthermore, a vibration of the specimens from Trial 3 showed to be beneficial considering the performed contact surface at ultimate load. Considering the W/C ratio, a reduction of the W/C-ratio to 0.62 (Mix 1) reduces the contact surface at ultimate load by 20.8 % for the vibrated specimens and by 43.8 % for the non-vibrated

ones (Table 10). These results were coherent to the analysis of the compressive strength in section 3.1.3.

4.2.3. Analysis of curing time of 28 days and stepwise loading

As previously stated and generally known, a curing time of 28d induces a higher compressive strength than a curing time of 14d for the masonry blocks. The same observation can be done for the contact surfaces, which increased in average for the three tested masonry blocks (MB 1_28-MB 3_28) from 72.2 % to 83.2 % (Fig. 17). These specimens showed identical contact surfaces on top and bottom of the masonry blocks, which implies that the filling technique is validated for both sides.

By applying a gradual load on top of the three masonry blocks (MB1_14d_g – MB3_14d_g), it is possible to study the relationship between the contact area and the compressive strength (Fig. 18). By loading and unloading the contact area was in average 80.6 % for the three masonry blocks and thus, 1.3 times higher than the contact surface achieved with a continuous loading (Trial 3 Table 10). The reason for a gradual load implying a higher contact surface at ultimate load is due to the movement of the fibres in the matrix, which indicates also a compacter matrix.

The relationship between the stress and the contact area that the block presents with the gradual load could be demonstrated through an exponential equation (Fig. 18) with a coefficient of determination (R^2) of 0.99. According to the analysis, the higher the applied compressive strength, the higher the percentage of contact between the surfaces. By inserting the load-bearing capacity achieved in Trial 3 (3.44 MPa in Table 8) into the exponential equation from Fig. 18, a theoretical contact
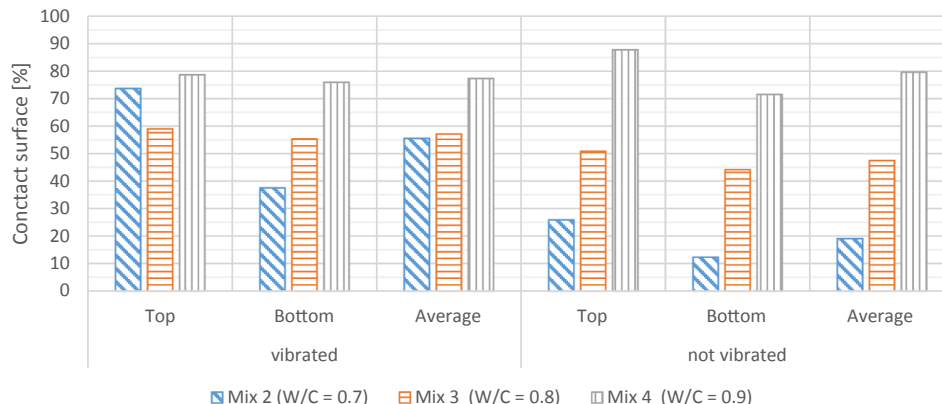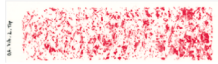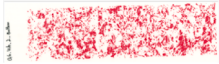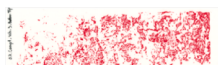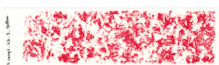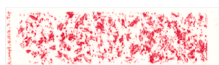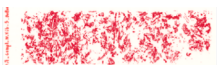

Fig. 16. Contact surface of the top and bottom at ultimate load of the masonry blocks from Trial 1 and their respective average.

Table 10

FUJIFILM strips showing the contact surface of one out of three masonry blocks for each vibrated and not vibrated mixture from Trial 3 as well as their contact surface in [%] and average in [%]

	vibrated			Not vibrated		
	Top	Bottom	Avg.	Top	Bottom	Avg.
Mix 1			57.2			34.2
	54.1	60.2		32.4	36.1	
Mix 2			72.2			60.9
	67.6	76.8		59.6	62.2	
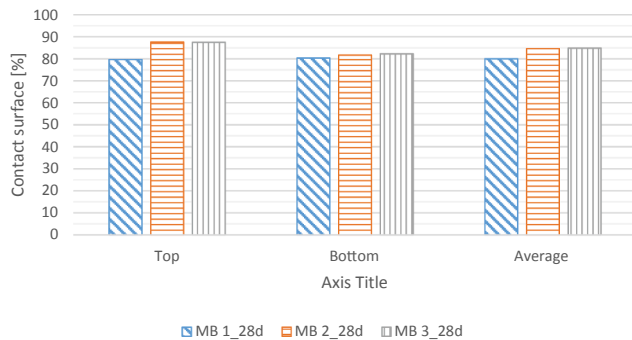
Fig. 17. Contact surface and average of the masonry blocks after a curing time of 28d (Trial 4).

of 67.9 % can be calculated, which is 6 % lower than the measured value (72.2 % from Table 10). Since a gradual loading implies a higher load-bearing capacity of the masonry block, the difference of 6 % originates from the duration of the loading test. Thus, the achieved compressive strength is dependent on the actual contact surface: the higher the contact surface the lower the amount of stress concentration peaks leaning to a reduction of crack formation.

4.2.4. Analysis on wallets

The contact surface at the horizontal joints (J1 and J2) of the Wallets 2 and 3 were similar with 55–59 % (Table 11). The vertical joints between each neighbouring masonry block are visible because no mortar was used between the blocks, so the roughness and height imperfections

could not be rectified, and this is visible in the contact strips. Furthermore, on both wallets, the pressure was distributed entirely over the whole area without any specific point concentration. It is also visible in Table 11 that the highest peak stresses (black dots at 3.0 MPa) were mostly in the middle part of the contact area.

In conclusion, the roughness of all models was constant for all masonry blocks created using the second moulding procedure and the height differences had a low standard deviation of $\mu = 0.285$ mm (Fig. 19). Furthermore, the low Young's Modulus from the mixtures (0.5 – 4.0 GPa) [33] reduces the impact of the roughness and the height differences on the contact surface, accordingly also on the load-bearing capacity. So, the low Young's Modulus is the reason for a coherent and constant contact between the masonry blocks of the wallets.

4.3. Height differences of the masonry blocks

The height of the masonry blocks was measured and categorised according to the mould in which they were produced. The mould presented in Fig. 4(b) was filled from the upper side of the block, which is also the surface on which the loading is later applied. By filling the mould from the side (Fig. 4(c)), the height of the masonry block is limited by the surface of the mould and is therefore more even. The masonry blocks based filled from the upper side generated a mean height of 202.78 mm and a standard deviation of 1.581 mm. Meanwhile, the masonry blocks established with a filling from the side surface achieved a mean height of 201.52 mm and a standard deviation of 0.285 mm. According to this data, a normal Gaussian distribution could be settled and both models could be compared. In Fig. 19, the probability density is presented as a function of the height variation of each masonry
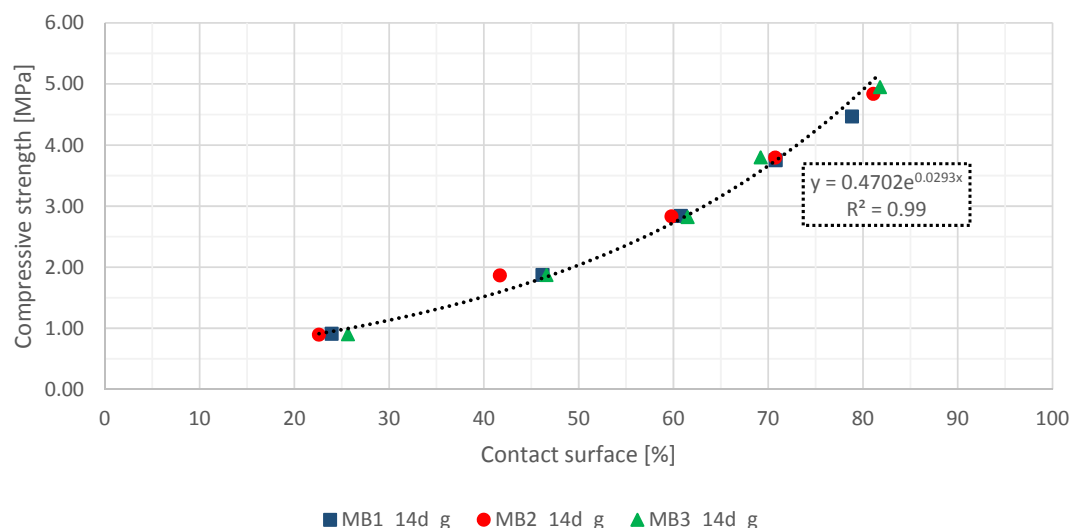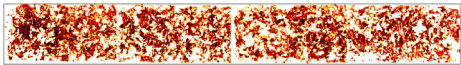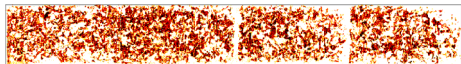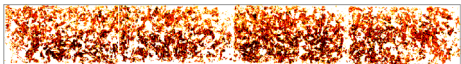

Fig. 18. Compressive strength in function of the contact surface from the three masonry blocks based on Mix 2 (Trial 4) at a curing time of 14d.

Table 11

Analysed strips showing the contact surface [%] for both horizontal joints of Wallet 2 and 3 at their respective load-bearing capacity and the point pressure in a scale from 0–3.0 MPa.

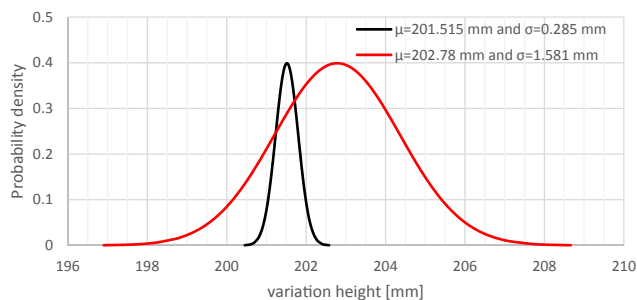| Position	Wallet 2 Contact surface [%]	Wallet 3 Contact surface [%]
J1	55.8	55.7
J2	58.5	58.6
[MPa]		

Fig. 19. Gaussian normal distribution of the height of the masonry blocks: in red the height variation when filling the mould from the upper side (Fig. 4 (b)) and in black when filling the mould from the side (Fig. 4 (c)). (For interpretation of the references to colour in this figure legend, the reader is referred to the web version of this article.)

block. The red curve represents the height variation of the masonry blocks which were based on the mould filled from the upper side (Fig. 4 (b)) and the black curve represents the masonry blocks generated using mould filled from the side (Fig. 4(c)). Hence, it can be concluded that filling the masonry block from the side (Fig. 4(c)) implies a reduction of the standard deviation of the heights of the masonry block by 82 %. Furthermore, it can be assumed that the standard deviation of the top and bottom surface's roughness of the masonry block is also improved by filling the masonry block from the side.

5. Conclusions

This study aimed to develop and analyse a Miscanthus concrete mixture experimentally for masonry blocks and dry-stacked walls. The height differences of the masonry blocks were considerably reduced by adapting the moulding procedure. Furthermore, the roughness was analysed by interpreting the contact surface at different tests. The conclusions of the treated points are summarised as follows:

- The impact of the vibration on the load-bearing capacity (LBC) of Miscanthus concrete was reduced with an increasing W/C-ratio. Mix 4 (W/C = 0.9) showed a reduction of 7 % in the LBC for the prisms but an increase of 12 % for the masonry blocks by omitting the vibration during the creation process.
- The mixing procedure of first creating a cement paste with the full amount of water and introduce the Miscanthus fibres as last showed to be the most suitable considering the LBC. Independent from the vibration state the specimens based on the mixing procedure B showed the highest LBC.

- The prisms from Mix 2 increased their LBC by 6 % with an increasing curing time from 14 to 28 d. A more important observation was performed on the masonry blocks, where a 57.5 % development could be experienced by increasing the curing time from 14 to 28 days.
- An exponential relation between the compressive strength and the contact surface could be established and be used to forecast the contact area of a masonry block. Nevertheless, a reduction of 6–12 % needs to be taken into consideration for a non-gradual loading.
- A cyclic loading on a single masonry block showed to increase its LBC by 25 %. The same procedure of loading showed to increase the LBC on the wallets by 15 %. These occurrences can be explained by the coefficient α_{cc} from a normal concrete, which includes the effects of the loading duration.
- The contact area in a wallet between two rows of masonry blocks showed to be between 55 and 59 %.

Finally, deducing from the results presented in this paper, the highest LBC was achieved using Mix 2 (W/C = 0.7) and the mixing procedure B. The contact surface of a single masonry block presented an exponential relation to the compressive strength. The joints of the dry-stacked wallets showed to achieve a contact surface of almost 60 % without any additional external layer between the blocks.

The obtained results of a Miscanthus lightweight concrete are promising considering an in-plane vertical loading. The shear resistance of the presented wallets can be assumed to be lower than the one of conventional walls. However, the out-of-plane flexural strength could be higher due to the fibrous masonry blocks which allow a higher energy absorption of the wallets. Furthermore, the presented results could be used as a foundation to analyse a possible degradation over time of the masonry block, which at this stage cannot be excluded. Finally, the last phase is the implementation of Miscanthus concrete masonry blocks from laboratory scale to mass production in industry. Knowing that the production of masonry blocks is done within a few seconds on special presses applying in parallel compaction and vibration with immediate demoulding afterwards, the adaptation of the mixture's rheology with an optimised choice of the water/cement ratio will be crucial. With these additional analyses, considering its ductile load-bearing behaviour, dry-stacked masonry based on Miscanthus concrete could become a sustainable solution allowing a deconstruction at end of life.

Declaration of Competing Interest

The authors declare that they have no known competing financial interests or personal relationships that could have appeared to influence the work reported in this paper.

References

[1] G. ABC. *2019 Global Status Report for Buildings and Construction*. 2019, Global Alliance for Buildings and Construction. 12.

[2] C. Maalouf, C. Ingrao, F. Scrucca, T. Moussa, A. Bourdot, C. Tricase, A. Presciutti, F. Asdrubali, An energy and carbon footprint assessment upon the usage of hemp-lime concrete and recycled-PET façades for office facilities in France and Italy, Journal of Cleaner Production 170 (2018) 1640–1653, https://doi.org/10.1016/j.jclepro.2016.10.111.

[3] G. Balčiūnas, S. Vėjelis, S. Vaitkus, A. Kairytė, Physical Properties and Structure of Composite Made by Using Hemp Hurds and Different Binding Materials, Procedia Engineering 57 (2013) 159–166, https://doi.org/10.1016/j.proeng.2013.04.023.

[4] M. Rubenstein, *Emissions from the Cement Industry,* 2012 [cited 2020]; Available from: https://blogs.ei.columbia.edu/2012/05/09/emissions-from-the-cement-industry/.

[5] OECD, *Global Material Resources Outlook to 2060: Economic Drivers and Environmental*. 2019, Paris: OECD Publishing, no.°p. 212, DOI: https://doi.org/10.1787/9789264307452-en.

[6] C. Niyigena, S. Amziane, and A. Chateauneuf. *Investigating Hemp Concrete Mechanical Properties Variability Due to Hemp Particles*. in *Mechanics of Composite and Multi-functional Materials, Volume 7*. 2017. Cham: Springer International Publishing DOI: https://doi.org/10.1007/978-3-319-41766-0_2.

[7] C.-F.-J. Kuo, C.-H. Lin, M.-W. Hsu, Analysis of intelligent green building policy and developing status in Taiwan, Energy Policy 95 (2016) 291–303, https://doi.org/10.1016/j.enpol.2016.04.046.

[8] F. Collet, M. Bart, L. Serres, J. Miriel, Porous structure and water vapour sorption of hemp-based materials, Construction and Building Materials 22 (6) (2008) 1271–1280, https://doi.org/10.1016/j.conbuildmat.2007.01.018.

[9] J. Figala, V. Vranová, K. Rejšek, and P. Formánek, *Giant Miscanthus (Miscantus x Giganteus Greef Et Deu.) – A Promising Plant for Soil Remediation: A Mini Review*. Acta Universitatis Agriculturae et Silviculturae Mendelianae Brunensis, 2015, vol. 63, p. 2241-2246, DOI: https://doi.org/10.11118/201563062241.

[10] H. Wang, P.-C. Chiang, Y. Cai, C. Li, X. Wang, T.-L. Chen, S. Wei, Q. Huang, Application of Wall and Insulation Materials on Green Building, *A Review*. Sustainability 10 (9) (2018) 3331, https://doi.org/10.3390/su10093331.

[11] M. Fourmentin, P. Faure, P. Pelupessy, V. Sarou-Kanian, U. Peter, D. Lesueur, S. Rodts, D. Daviller, P. Coussot, NMR and MRI observation of water absorption/uptake in hemp shives used for hemp concrete, Construction and Building Materials 124 (2016) 405–413, https://doi.org/10.1016/j.conbuildmat.2016.07.100.

[12] S. Agaajani, *Development and investigation of a new dry-stacked wall system*. Doctoral Dissertation, 2015, University of Luxembourg: Luxembourg. Available from: http://hdl.handle.net/10993/21575.

[13] I. Lewandowski, J. Clifton-Brown, A. Kiesel, A. Hastings, et al., *2 – Miscanthus*, in *Perennial Grasses for Bioenergy and Bioproducts*, E. Alexopoulou, Editor. 2018, Academic Press. p. 35-59 DOI: https://doi.org/10.1016/B978-0-12-812900-5.00002-3.

[14] I. Lewandowski, J.C. Clifton-Brown, J.M.O. Scurlock, W. Huisman, Miscanthus: European experience with a novel energy crop, Biomass and Bioenergy 19 (4) (2000) 209–227, https://doi.org/10.1016/S0961-9534(00)00032-5.

[15] J. Clifton-Brown, A. Hastings, M. Mos, J.P. McCalmont, C. Ashman, D. Awty-Carroll, J. Cerazy, Y.-C. Chiang, S. Cosentino, W. Cracroft-Eley, J. Scurlock, I. S. Donnison, C. Glover, I. Gołąb, J.M. Greef, J. Gwyn, G. Harding, C. Hayes, W. Helios, T.-W. Hsu, L.S. Huang, S. Jeżowski, D.-S. Kim, A. Kiesel, A. Kotecki, J. Krzyzak, I. Lewandowski, S.H. Lim, J. Liu, M. Loosely, H. Meyer, D. Murphy-Bokern, W. Nelson, M. Pogrzeba, G. Robinson, P. Robson, C. Rogers, G. Scalici, H. Schuele, R. Shafiei, O. Shevchuk, K.-U. Schwarz, M. Squance, T. Swaller, J. Thornton, T. Trucksess, V. Botnari, I. Vizir, M. Wagner, R. Warren, R. Webster, T. Yamada, S. Youell, Q. Xi, J. Zong, R. Flavell, Progress in upscaling Miscanthus biomass production for the European bio-economy with seed-based hybrids, GCB Bioenergy 9 (1) (2017) 6–17, https://doi.org/10.1111/gcbb.2017.9.issue-110.1111/gcbb.12357.

[16] D.G. Christian, A.B. Riche, N.E. Yates, Growth, yield and mineral content of Miscanthus×giganteus grown as a biofuel for 14 successive harvests, Industrial Crops and Products 28 (3) (2008) 320–327, https://doi.org/10.1016/j.indcrop.2008.02.009.

[17] K. Głowacka, A review of the genetic study of the energy crop Miscanthus, Biomass and Bioenergy 35 (7) (2011) 2445–2454, https://doi.org/10.1016/j.biombioe.2011.01.041.

[18] B. Barbosa, S. Boléo, S. Sidella, J. Costa, M.P. Duarte, B. Mendes, S.L. Cosentino, A. L. Fernando, Phytoremediation of Heavy Metal-Contaminated Soils Using the Perennial Energy Crops Miscanthus spp. and Arundo donax L, BioEnergy Research 8 (4) (2015) 1500–1511, https://doi.org/10.1007/s12155-015-9688-9.

[19] V. Pidlisnyuk, T. Stefanovska, E.E. Lewis, L.E. Erickson, L.C. Davis, Miscanthus as a Productive Biofuel Crop for Phytoremediation, Critical Reviews in Plant Sciences 33 (1) (2014) 1–19, https://doi.org/10.1080/07352689.2014.847616.

[20] N. Bilandžija. *Perspective and potential use of Miscanthus x Giganteus Culture in Croatia*. in *13th international waste management symposium*. 2014. Zagreb.

[21] T.B. Voigt, Are the environmental benefits of Miscanthus × giganteus suggested by early studies of this crop supported by the broader and long-term contemporary studies? GCB Bioenergy 7 (4) (2015) 567–569, https://doi.org/10.1111/gcbb.2015.7.issue-410.1111/gcbb.12150.

[22] U. Jørgensen, Benefits versus risks of growing biofuel crops: the case of Miscanthus, Current Opinion in Environmental Sustainability 3 (1) (2011) 24–30, https://doi.org/10.1016/j.cosust.2010.12.003.

[23] Miscanthus.de and R. Pude, *Verwertungsvielfalt von Miscanthus* 2012 [cited 2020]; Available from: http://miscanthus.de/verwertung.html.

[24] R. Pude, C.H. Treseler, R. Trettin, G. Noga, Suitability of Miscanthus Genotypes for Lightweight Concrete, Die Bodenkultur – Journal for Land Management, Food and Environment 56 (1/4) (2005) 61–69.

[25] C. Godard, J. Boissy, B. Gabrielle, Life-cycle assessment of local feedstock supply scenarios to compare candidate biomass sources, GCB Bioenergy 5 (1) (2013) 16–29, https://doi.org/10.1111/gcbb.2012.5.issue-110.1111/j.1757-1707.2012.01187.x.

[26] S. Wang, S. Wang, A. Hastings, M. Pogson, P. Smith, Economic and greenhouse gas costs of Miscanthus supply chains in the United Kingdom, GCB Bioenergy 4 (3) (2012) 358–363, https://doi.org/10.1111/gcbb.2012.4.issue-310.1111/j.1757-1707.2011.01125.x.

[27] K.B. Anand, K. Ramamurthy, Development and Performance Evaluation of Interlocking-Block Masonry, Journal of Architectural Engineering 6 (2) (2000) 45–51, https://doi.org/10.1061/(ASCE)1076-0431(2000)6:2(45).

[28] M. Martínez, S. Atamturktur, Experimental and numerical evaluation of reinforced dry-stacked concrete masonry walls, Journal of Building Engineering 22 (2019) 181–191, https://doi.org/10.1016/j.jobe.2018.12.007.

[29] M. Kohail, H. Elshafie, A. Rashad, H. Okail, Behavior of post-tensioned dry-stack interlocking masonry shear walls under cyclic in-plane loading, Construction and Building Materials 196 (2019) 539–554, https://doi.org/10.1016/j.conbuildmat.2018.11.149.

[30] G.G. Chewe Ngapeya, D. Waldmann, F. Scholzen, Impact of the height imperfections of masonry blocks on the load bearing capacity of dry-stack masonry walls, Construction and Building Materials 165 (2018) 898–913, https://doi.org/10.1016/j.conbuildmat.2017.12.183.

[31] G.G. Chewe Ngapeya, D. Waldmann, *Experimental and analytical analysis of the load-bearing capacity Pu of improved dry-stacked masonry*. Journal of Building, Engineering 27 (2020) 100927, https://doi.org/10.1016/j.jobe.2019.100927.

[32] G. Vasconcelos, P.B. Lourenço, Experimental characterization of stone masonry in shear and compression, Construction and Building Materials 23 (11) (2009) 3337–3345, https://doi.org/10.1016/j.conbuildmat.2009.06.045.

[33] P. Pereira Dias, D. Waldmann, Optimisation of the mechanical properties of Miscanthus lightweight concrete, Construction and Building Materials 258 (2020) 119643–119656, https://doi.org/10.1016/j.conbuildmat.2020.119643.

[34] C. members, *EN1996-1-1:2005, Eurocode 6 – Design of masonry structures – Part 1-1: General rules for reinforced and unreinforced masonry structures*. 2005.

[35] G.G. Chewe Ngapeya, D. Waldmann, Overcome of bed-joint imperfections and improvement of actual contact in dry-stacked masonry, Construction and Building Materials 233 (2020) 117173, https://doi.org/10.1016/j.conbuildmat.2019.117173.

[36] J. A. Greenwood and J. B. P. Williamson, *Contact of nominally flat surfaces*. Proceedings of the Royal Society A: Mathematical, Physical and Engineering Sciences, 1966, DOI: https://doi.org/10.1098/rspa.1966.0242.

[37] Y. Yin, Y. Fan, Influence of Roughness on Shear Bonding Performance of CFRP-Concrete Interface, Materials 11 (10) (2018) 1875, https://doi.org/10.3390/ma11101875.

[38] E. C. f. standardization, *Cement -Part 1: Composition, specifications and conformity criteria for common cements*, in *DIN EN 197-1:2011-11 Cement -Part 1: Composition, specifications and conformity criteria for common cements*. 2011.

[39] G.H. Tattersall, P.H. Baker, The effect of vibration on the rheological properties of fresh concrete, Magazine of Concrete Research 40 (143) (1988) 79–89, https://doi.org/10.1680/macr.1988.40.143.79.

[40] FUJIFILM, *Fujifilm's measurement film solution – Structure and principle,* 2020 [cited 2020]; Available from: https://www.fujifilm.com/products/measurement_film/en/prescale/feature/.

[41] Nadezda Stevulova, Julia Cigasova, Pavol Purcz, Ivana Schwarzova, Frantisek Kacik, Anton Geffert, Water Absorption Behavior of Hemp Hurds Composites, Materials 8 (5) (2015) 2243–2257, https://doi.org/10.3390/ma8052243.

[42] H.N. Dhakal, Z.Y. Zhang, M.O.W. Richardson, Effect of water absorption on the mechanical properties of hemp fibre reinforced unsaturated polyester composites, Composites Science and Technology 67 (7) (2007) 1674–1683, https://doi.org/10.1016/j.compscitech.2006.06.019.

[43] A. Célino, S. Fréour, F. Jacquemin, P. Casari, Characterization and modeling of the moisture diffusion behavior of natural fibers, Journal of Applied Polymer Science 130 (1) (2013) 297–306, https://doi.org/10.1002/app.39148.

[44] P.L. Domone, Self-compacting concrete: An analysis of 11 years of case studies, Cement and Concrete Composites 28 (2) (2006) 197–208, https://doi.org/10.1016/j.cemconcomp.2005.10.003.

[45] S. Elfordy, F. Lucas, F. Tancret, Y. Scudeller, L. Goudet, Mechanical and thermal properties of lime and hemp concrete ("hempcrete") manufactured by a projection

process, Construction and Building Materials 22 (10) (2008) 2116–2123, https://doi.org/10.1016/j.conbuildmat.2007.07.016.

[46] L. Arnaud, E. Gourlay, Experimental study of parameters influencing mechanical properties of hemp concretes, Construction and Building Materials 28 (1) (2012) 50–56, https://doi.org/10.1016/j.conbuildmat.2011.07.052.

[47] L. Courard, V. Parmentier, Carbonated Miscanthus mineralized aggregates for reducing environmental impact of lightweight concrete blocks, Sust. Build. 2 (2017) 9, https://doi.org/10.1051/sbuild/2017004.

[48] V. Picadet, in: Bulk Density and Compressibility, in Bio-aggregates Based Building Materials, Springer, Dordrecht, 2017, pp. 111–124, https://doi.org/10.1007/978-94-024-1031-0.

[49] I. Merta, E.K. Tschegg, Fracture energy of natural fibre reinforced concrete, Construction and Building Materials 40 (2013) 991–997, https://doi.org/10.1016/j.conbuildmat.2012.11.060.

[50] S. Pavía, in: *Effect of Testing Variables (Method of Production)*, in *Bio-aggregates Based Building Materials : State-of-the-Art Report of the RILEM Technical Committee 236-BBM*, Dordrecht, Springer, Netherlands, 2017, pp. 189–201, https://doi.org/10.1007/978-94-024-1031-0_9.

[51] C. Juárez, B. Guevara, P. Valdez, A. Durán-Herrera, Mechanical properties of natural fibers reinforced sustainable masonry, Construction and Building Materials 24 (8) (2010) 1536–1541, https://doi.org/10.1016/j.conbuildmat.2010.02.007.

[52] E. Awwad, D. Choueiter, H. Khatib, Concrete Masonry Blocks Reinforced with Local Industrial Hemp Fibers and Hurds, Kyoto Research Park, Kyoto, Japan, 2013.

[53] E. Bernat, L. Gil, P. Roca, C. Sandoval, Experimental and numerical analysis of bending–buckling mixed failure of brickwork walls, Construction and Building Materials 43 (2013) 1–13, https://doi.org/10.1016/j.conbuildmat.2013.01.025.

[54] E. C. f. standardisation, *Section 3.1.6: Design compressive and tensile strengths*, in *EN1992: Design of concrete structures – Part 1-1: General rules and rules for buildings*. 2004: Brussels.

[55] M.Z. Cohn, M. Bartlett, Computer-simulated flexural tests of partially prestressed concrete sections, Journal of the Structural Division 108 (12) (1982) 2747–2765.

[56] Lan Dong, J.C.M. Kao, W.-P. Sung, Study on Seismic Behavior of Recycled Concrete Energy-efficient Homes Structure Wall, MATEC Web of Conferences 63 (2016) 03016, https://doi.org/10.1051/matecconf/20166303016.

[57] P. Lourenco, G. Vasconcelos, J. Gouveia, V. Haach, et al., *Validation of masonry systems for in-plane lateral loading using truss reinforcement*, in *14th International Brick and Block Masonry Conference*, I.M. 2008, Editor. 2008, IB2MAC 2008: Sydney, Australia.

[58] Mehrollah Rakhshanimehr, M. Reza Esfahani, M. Reza Kianoush, B. Ali Mohammadzadeh, S. Roohollah Mousavi, Flexural ductility of reinforced concrete beams with lap-spliced bars, Canadian Journal of Civil Engineering 41 (7) (2014) 594–604, https://doi.org/10.1139/cjce-2013-0074.

[59] Xudong Chen, Yebo Huang, Chen Chen, Jun Lu, Xiangqian Fan, Experimental study and analytical modeling on hysteresis behavior of plain concrete in uniaxial cyclic tension, International Journal of Fatigue 96 (2017) 261–269, https://doi.org/10.1016/j.ijfatigue.2016.12.002.

[60] R. G. Drysdale, R. Vanderkeyl, and A. A. Hamid, *Shear Strength of Brick Masonry Joints* in *Vth International Brick Masonry Conference*. 1979, IB2MAC 1979: Washington D.C., U.S.A. p. 106-113.

[61] S. Hamoush, M. McGinley, P. Mlakar, M.J. Terro, Out-of-plane behavior of surface-reinforced masonry walls, Construction and Building Materials 16 (6) (2002) 341–351, https://doi.org/10.1016/S0950-0618(02)00024-7.